World Academy of Science, Engineering and Technology
International Journal of Chemical and Materials Engineering
Vol:18, No:5, 2024

First-Principle Investigation of the Electronic Band Structure and Dielectric Response Function of $ZnIn_2Se_4$ and $ZnIn_2Te_4$

Nnamdi N. Omehe, Chibuzo Emeruwa

Open Science Index, Chemical and Materials Engineering Vol:18, No:5, 2024 publications.waset.org/10013650.pdf

Abstract**—**$ZnIn_2Se_4$ and $ZnIn_2Te_4$ are vacancy defect materials whose properties have been investigated using Density Functional Theory (DFT) framework. The pseudopotential method in conjunction with the LDA+U technique and the Projector Augmented Wave (PAW) was used to calculate the electronic band structure, total density of state, and the partial density of state; while the norm-conserving pseudopotential was used to calculate the dielectric response function with scissors shift. Both $ZnIn_2Se_4$ and $ZnIn_2Te_4$ were predicted to be semiconductors with energy band gap of 1.66 eV and 1.33 eV respectively, and they both have direct energy band gap at the gamma point of high symmetry. The topmost valence subband for $ZnIn_2Se_4$ and $ZnIn_2Te_4$ has an energy width of 5.7 eV and 6.0 eV respectively. The calculations of partial density of state (PDOS) show that for $ZnIn_2Se_4$, the top of the valence band is dominated by Se-4p orbital, while the bottom of the conduction band is composed of In-5p, In-5s, and Zn-4s states. PDOS for $ZnIn_2Te_4$, shows that the top of the valence band is mostly of Te-5p states, while its conduction band bottom is composed mainly of Zn-4s, Te-5p, Te-5s, and In-5s states. Dielectric response function calculation yielded (0) of 11.9 and 36 for $ZnIn_2Se_4$ and $ZnIn_2Te_4$ respectively.

Keywords**—**Optoelectronic, Dielectric Response Function, LDA+U, band structure calculation.

I. Introduction

THE materials $ZnIn_2Se_4$ and $ZnIn_2Te_4$ are members of group II-III-VI_4 family of ternary vacancy defect Chalcopyrite semiconductors. Their technological applicability has attracted researcher's attention. They find applications in opto-electronics, photovoltaics, switching memory [1]-[5], photocatalytic evolution of hydrogen [6], and thermionic devices [7]. These materials have been previously investigated experimentally and theoretically.

Experimentally, Trah and Kramer [8] prepared samples of $ZnIn_2Se_4$ via its elemental components, and analysis revealed lattice parameters of a = 5.7095 Å, c = 11.449 Å, and 8i Wyckoff site coordinate (0.23,0.23, 0.384). $ZnIn_2Se_4$ (ZISe) was reported by Marsh and Robinson [9] to belong to the I-42m space group. Razzett et al. [10] prepared layered samples of $ZnIn_2S_4$ and $ZnIn_2Se_4$. These samples were analysed via X-ray diffraction, atomic absorption spectroscopy, and Raman scattering. They observed disordered structure. Riede et al. [11] reported on the vibrational properties of $ZnIn_2Se_4$ from Raman studies. Thermal properties of $ZnIn_2Se_4$ have been mentioned in the literature [12]. Polycrystalline nanostructures of $ZnIn_2Se_4$ were synthesized [13] by thermal evaporation. The optical properties of the samples were found to be thickness independent, and that there were two transition types in the prepared samples: direct transition with energy band gap of 1.76 eV and indirect with energy band gap of 2.3 eV. References [12] and [13] also reported $\varepsilon(\infty) = 6.84$ and $\varepsilon(0) = 8.17$. Babu et al. [14] investigated the effect of precursor concentration on the properties of synthesized $ZnIn_2Se_4$ samples, a band gap range of 2.91 eV to 3.05 eV was observed. Heterojunction diode of $ZnIn_2Se_4$ and silicon has been fabricated [15], [16]. Khawar et al. [17] have reported on the cubic phase of $ZnIn_2Se_4$. Patel and Ali [18] prepared bulk and thin film samples of $ZnIn_2Te_4$ by melting method using Transmission Electron Microscopy (TEM) and x-ray diffraction to characterize the samples.

The Bridgman method was used by Ozaki and Adachi [19] to grow samples of $ZnIn_2Te_4$ that were then analysed via optical absorption, spectroscopic ellipsometry, and X-ray photoelectron spectroscopy; their characterization revealed a direct band of 1.4 eV and an $\varepsilon_1(0)$ value of about 6.0. The thermal conductivity of vacancy defect chalcopyrite $ZnIn_2Te_4$ material was reported by Suriwong et al. [20]. The cubic phase of $ZnIn_2Te_4$, has been reported in the literature [21], the DFT calculations show that cubic $ZnIn_2Te_4$ has a band gap of about 1.4 eV. $ZnIn_2Te_4$ glass studied by Shakra et al. [22], the glass was prepared by melting, and gradual cooling of the samples. Ganguli et al. [23] in their DFT study of the electronic and optical properties of $ZnIn_2Te_4$ used the TB-LMTO method, result of the investigations showed that $ZnIn_2Te_4$ is a direct band gap semiconductor with a fundamental gap value of 1.37 eV. Similarly, Ayeb et al. [24] in their DFT work using the FLAPW; and Pseudopotential methods [25] reported band gap values of 1.2 eV and 0.836 eV respectively. They also reported on the linear and nonlinear optical properties of $ZnIn_2Te_4$ [25]. Reguiey et al. [26] used FPLAPW method to investigate the thermodynamic and optical properties of $ZnIn_2Se_4$ and $ZnIn_2Te_4$. The nature of the vacancy defect in $Z_nIn_2Te_4$ was reported by Wu et al. [27].

In the present work, the DFT+U method would be applied to study the electronic and optical properties of $ZnIn_2Se_4$ and $ZnIn_2Te_4$ compounds.

N. N. Omehe is with the Department of Physics, Federal University Otuoke, Bayelsa State, Nigeria (phone: +2347031003831; omehenn@fuotuoke.edu.ng).

C. Emeruwa was with Veritas University Abuja, Nigeria. He is now with the Department of Physics, Federal University Otuoke, Bayelsa State, Nigeria (e-mail: emeruwacc@fuotuoke.edu.ng).

Open Science Index, Chemical and Materials Engineering Vol:18, No:5, 2024 publications.waset.org/10013650.pdf

II. Computational Details

$ZnIn_2Se_4$ and $ZnIn_2Te_4$ are vacancy defect chalcopyrite materials with the 1-42m space group. The vacancy is at the (0.0, 0.0, 0.5) 2b Wyckoff site. The atomic positions and the 8i atomic coordinates used in this investigation were taken from [28]. The defect chalcopyrite structure has two formula unit in per unit cell, a total of fourteen atoms; eight selenium/tellurium (Se/Te), four indium (In) and two Zinc (Zn) atoms. The quantum software code, the Abinit [29], [30] was utilized in the calculations. The electronic band structure, the total and PDOS and the dielectric response function will be computed in this work. Table I shows the input variable of the materials structure used in the calculations. The LDA+U scheme, which includes the coulombs interaction term U, for d- electrons was used in the study to calculated the electronic band structure and density of state. This scheme uses the Projector Augmented Were (PAW) as the Pseudopotential. The dielectric functions were calculated using norm-conserving pseudopotential. The self-consistency calculations have energy tolerance of 10^{-6}, a kinetic energy cutoff of 12 Ha, and a 256 K-point mesh for brillouin zone integration. The following orbitals were included in the valence state of the respective atoms: Zn-3d, Zn-4s, In-4d, In-5p, In-5s, Se-4p, Se-4s, Te-5p, and Te-5s.

III. Results and Discussion

The electronic band structures of $ZnIn_2Se_4$ and $ZnIn_2Te_4$ have been computed and the result is presented in Figs. 1 (a) and (b) respectively. The plot is energy (eV) against high symmetry point of first brillouin zone, the direction of the plot is in Γ-X-M-P-Γ-M. The band structure of $ZnIn_2Se_4$ is presented in Fig. 1 (a), the Fermi energy E_F is indicated by the dash line. From Fig. 1 (a), the calculation showed $ZnIn_2Se_4$ to have semiconducting property. The conduction band minimum (CBM) and the valence band maximum (VBM) occur at the Γ-point of high symmetry. The calculated energy band gap is 1.66 eV, which agrees with experimental value of 1.68 eV [28]. The subband at the top of the valence band has an energy width of 5.7 eV, the intra valence band gap between the first and second subband is 5.9 eV, and the second subband has an energy window of about 1.3 eV. The electronic band structure of $ZnIn_2Te_4$ is shown in Fig. 1 (b). The material is predicted to have semiconducting properties with a direct band gap occurring at the Γ- point. The calculated value of the gap is 1.33 eV, which is comparable to experimental result [28] and results from previous calculations [23]-[25]. The topmost subband has an energy width of 6.0 eV. The second subband is separated by a gap of 4.4 eV, and the width of the second subband is shown to be 1.5 eV.

TABLE I
THE STRUCTURAL INPUT USED IN THE CALCULATIONS

Material	a(Å)	C(Å)	x	y	z
$ZnIn_2Se_4$	5.69	11.40	0.25	0.25	0.125
$ZnIn_2Se_4$	6.11	12.20	0.25	0.25	0.125

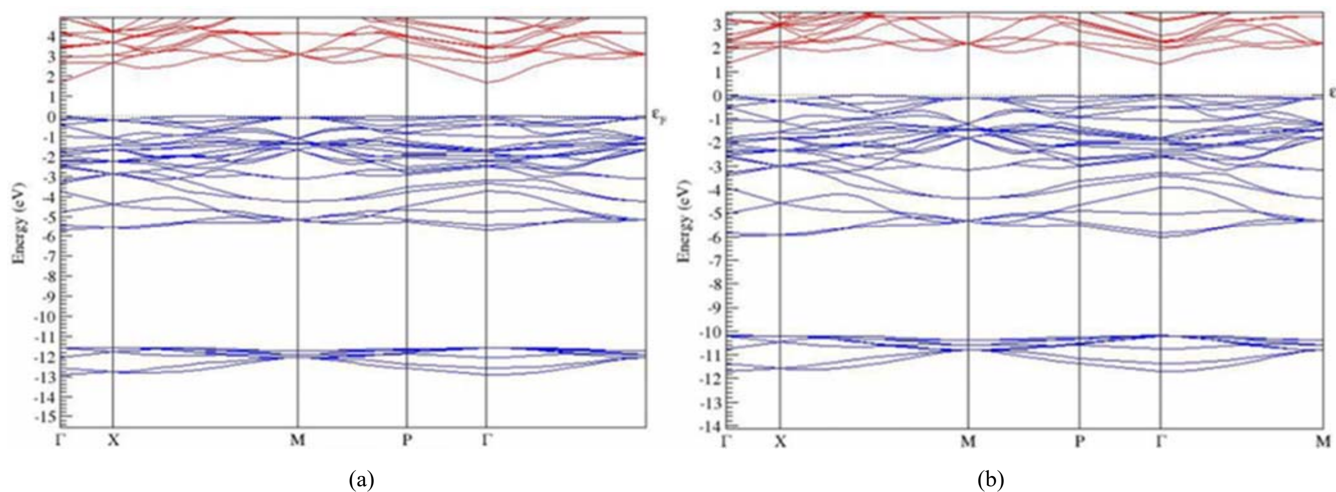

(a) (b)

Fig. 1 The Electronic band structure of (a) $ZnIn_2Se_4$, (b) $ZnIn_2Te_4$

The total density of state (TDOS) for $ZnIn_2Se_4$ and $ZnIn_2Te_4$ is presented in Figs. 2 (a) and (b) respectively. The density of state (DOS) is plotted against energy (Ha). The features or peaks in the plots represent the decomposed orbital contributions to TDOS. Fig. 2 (a) shows all the subbands in the electronic band structure of $ZnIn_2Se_4$. The Fermi level is at 0.2 Ha, and there are six valence subbands separable by varying degree of intra-valence band gap. Fig. 2 (b) displays the TDOS for $ZnIn_2Te_4$. The Fermi level is at -0.1 Ha. The various valence subbands are represented by the sharp peaks and curves. The conduction band is the feature from 0.0 Ha and beyond.

The PDOS for $ZnIn_2Se_4$ are displayed in Figs. 3-5. These plots represent the orbital decomposition for Zn, In, Se respectively. Fig. 3 shows the various Zinc's orbital contribution to the density of state of $ZnIn_2Se_4$. The Zn-3d states are shown in black while the Zn-4s is shown in red. The Zn-3d states are at a lower energy, and are concentrated at -0.65 Ha. The Zn-4s state is well dispersed and can be seen at -0.3 Ha, between -0.1 Ha to 0.1 Ha, and the bottom of the conduction band.

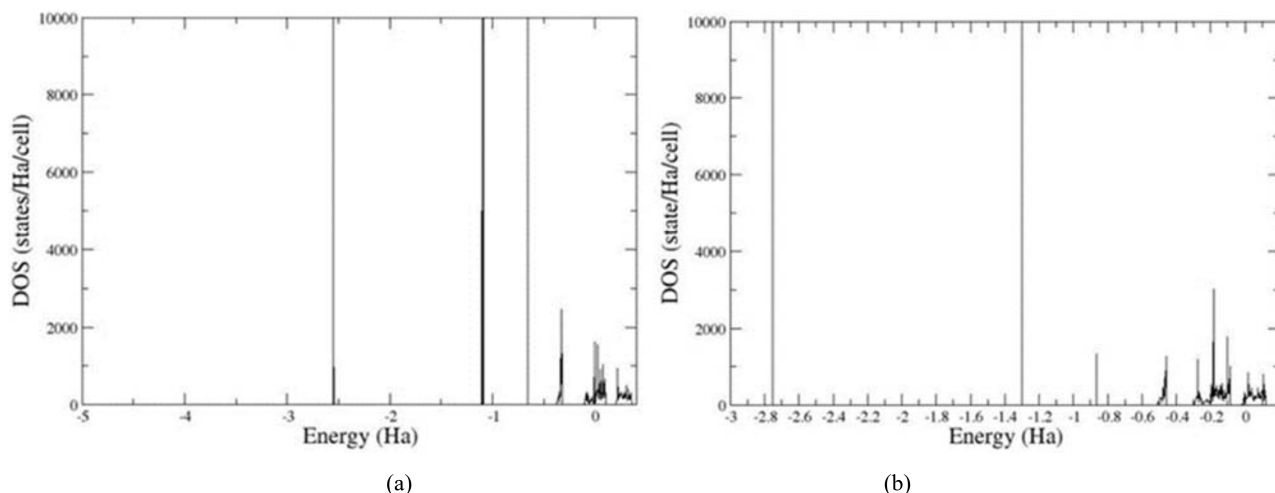

(a) (b)

Fig. 2 The total density of state of (a) $ZnIn_2Se_4$, (b) $ZnIn_2Te_4$

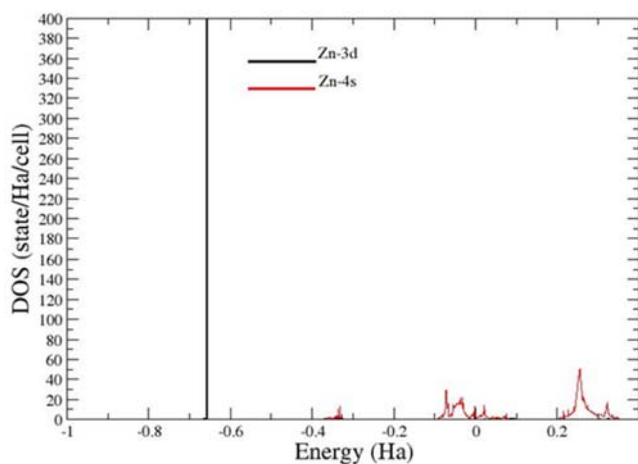

Fig. 3 The PDOS of Zn atom in $ZnIn_2Se_4$

Fig. 4 shows the various indium's orbitals contribution to TDOS. The In-4d state is depicted in black lines, In-5p in red lines, and In-5s in green lines. The feature at -1.1 Ha is the contribution from In-4d states. A very small portion of In-4d is also present in the conduction band. The feature between -0.4 and -0.2 Ha is made of up of In-5s and In-5p. The topmost valence subband is composed of In-5s and In-5p, with In-5p state at the top of the valence band. The conduction band shows an overlap of the three states in the indium atom.

The contributions from the selenium atom to TDOS comes from Se-4p and Se-4s, these are depicted in Fig. 5 by black and red lines respectively. Contributions from Se-4p are the dominated states at the top of the valence band while the preceding subband is entirely of Se-4s states. The conduction band is an overlap of both states. For $ZnIn_2Se_4$, the top of the valence band is dominated by Se-4p, while the bottom of the conduction band is composed mainly of In-5p, In-5s, and Zn-4a states.

The contributions from the various atoms in $ZnIn_2Te_4$ to TDOS are shown in Figs. 6-8. The orbital contributions from the Zinc atom are shown in Fig. 6. The Zinc's contribution in $ZnIn_2Te_4$ is similar to Zinc's contribution in $ZnIn_2Se_4$. The Zn-3d states are indicated in black lines while Zn-4s is in red. The Zn-3d states are concentrated at -0.86 Ha. Zn-4s has a large energy width, indicating a well dispersed state.

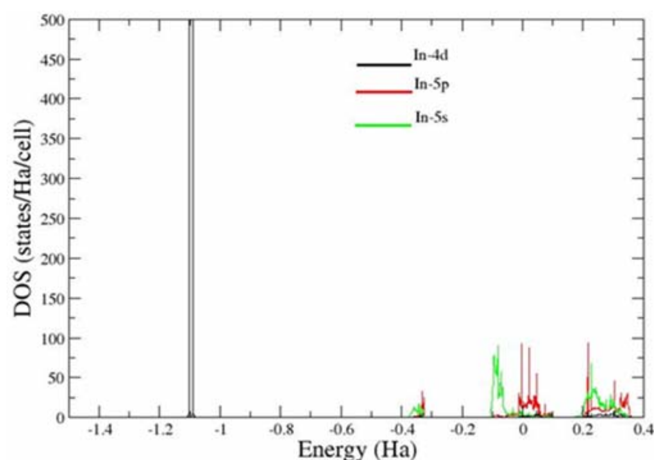

Fig. 4 The PDOS of Indium in $ZnIn_2Se_4$

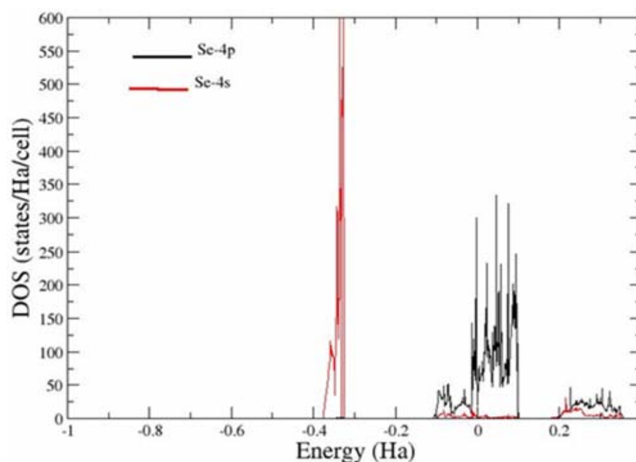

Fig. 5 The PDOS of Se in $ZnIn_2Se_4$

Open Science Index, Chemical and Materials Engineering Vol:18, No:5, 2024 publications.waset.org/10013650.pdf

Open Science Index, Chemical and Materials Engineering Vol:18, No:5, 2024 publications.waset.org/10013650.pdf

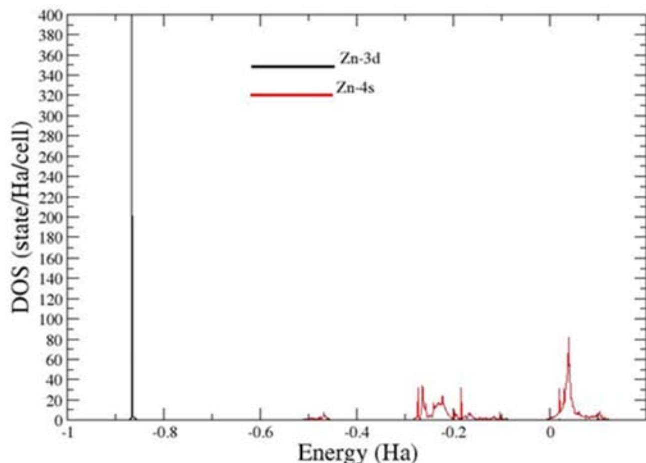

Fig. 6 The PDOS of Zn atom in $ZnIn_2Te_4$

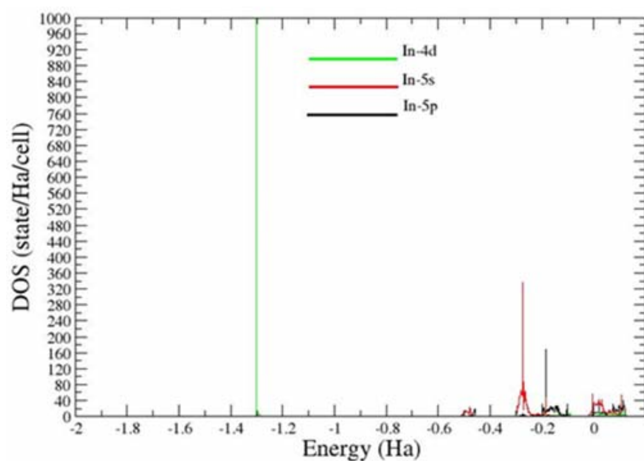

Fig. 7 The PDOS of Indium in $ZnIn_2Te_4$

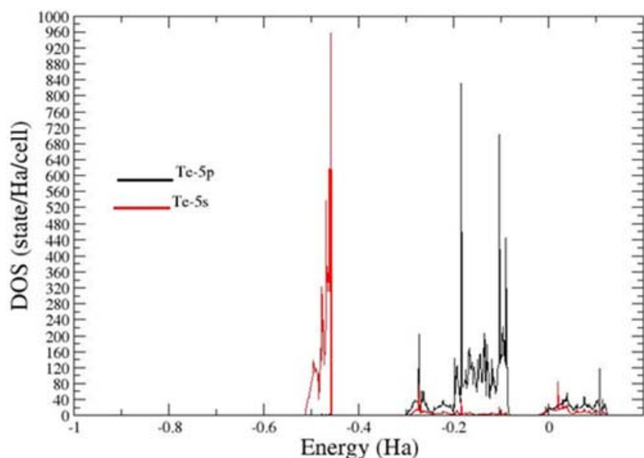

Fig. 8 The PDOS of Te in $ZnIn_2Te_4$

Fig. 7 presents the contributions from the various Indium valence orbitals included in the computations, these are In-4d, In-5s, In-5p, represented by green, red, and black lines respectively. The conduction band is composed of the three orbitals overlapping. The In-5p states dominates the top of the valence band with In-5s trialing. The bulk of Zn-4d states are concentrated at – 1.3 Ha.

The contribution from Te is shown in Fig. 8, and it is qualitatively and quantitatively similar to Se's contribution in $ZnIn_2Se_4$. The Te-5p orbitals dominate the top of the valence band while Te-5s state is shown about -0.5 Ha. The conduction band is an overlap of both orbitals. So, for $ZnIn_2Te_4$, the top of the valence band is mostly of Te-5p states, while its conduction band bottom is composed mainly of Zn-4s, Te-5p, Te-5s, and In-5s states.

IV. Optical Property

The dielectric function is at the centre of optical responses, it is a complex function expressed as $\varepsilon(\omega) = \varepsilon_1(\omega) + i\ \varepsilon_2(\omega)$; where $\varepsilon_1(\omega)$ is the real component and $\varepsilon_2(\omega)$ is the imaginary component. The graphical representation of $\varepsilon_1(\omega)$ and $\varepsilon_2(\omega)$ against energy for $ZnIn_2Se_4$, are shown in Figs. 9 (a) and (b) respectively. The peaks indicate critical points that are transition points in the band structure of the compound. The scissors shift was applied to the computation of the dielectric function, so that the onset of the first peak indicates the energy band gap. Fig. 9 (a) shows two major peaks A and B having energies 1.9 eV and 2.1 eV respectively. There is a shoulder C corresponding to $\varepsilon_1(\omega) = 2$ and at 2.4 eV. There is a steep descend of $\varepsilon_1(\omega)$ to -4 at 2.6 eV. From 2.9 eV, $\varepsilon_1(\omega)$ ascended from -3 to 7 at D corresponding to 3.4 eV. The energy interval from 3.4 eV to about 4.0 eV, shows three small peaks denoted by D, E, and F. $\varepsilon_1(\omega)$ is characterized by small peaks and humps between 4.2 eV and 8.0 eV. $\varepsilon_1(0)$ is found to be 11.9. The highest peak of $\varepsilon_1(\omega)$ is about 29 at 1.9 eV. The imaginary component $\varepsilon_2(\omega)$ is plotted against energy in eV and it is shown in Fig. 9 (b). Here, as in Fig. 9 (a), the first peak corresponds to the electron transition at the edge of the energy band gap. The first peak, which is like a shoulder shown as A corresponds to 1.9 eV, there are two peaks B and C at 2.0 eV and 2.2 eV respectively. A small shoulder D corresponds to 2.6 eV, then $\varepsilon_2(\omega)$ goes down to about 2.5 at 3.2 eV. It picks up and climbs to 12.5 at 4.2 eV. There is a peak G at 4.2 eV having two small shoulders E. and F. Other energy levels range from 4.2 eV to 8.0 eV and they have other small peaks and bumps similar to $\varepsilon_1(\omega)$.

The real and imaginary components of $ZnIn_2Te_4$plotted against energy are displayed in Figs. 10 (a) and (b) respectively. Fig. 10 (a) shows a single major peak at 3.3 eV. (ω) goes down steeply from 144 at A to about -18 at 1.6 eV at B, it goes down further from -18 to -42 before climbing to C at 2.0 eV. The transition points C, D, E, F, G, and H are bumps at 2.0 eV, 2.2 eV, 2.4 eV, 3.0 eV, 3.2 eV, 3.4 eV, and 3.6 eV respectively. (0) is seen to be about 36, and A corresponds to the highest peak at (ω) = 150. Fig. 10 (b) shows the plot (ω) against energy for $ZnIn_2Te_4$.The onset of transition is at 1.6 eV. The shoulder B is attached to A at 1.8 eV. C and D are small peaks at 2.0 eV and 2.2 eV. E, F, G, H and bumps at 2.5 eV, 3.2 eV, 3.4 eV, and 3.7

eV respectively.

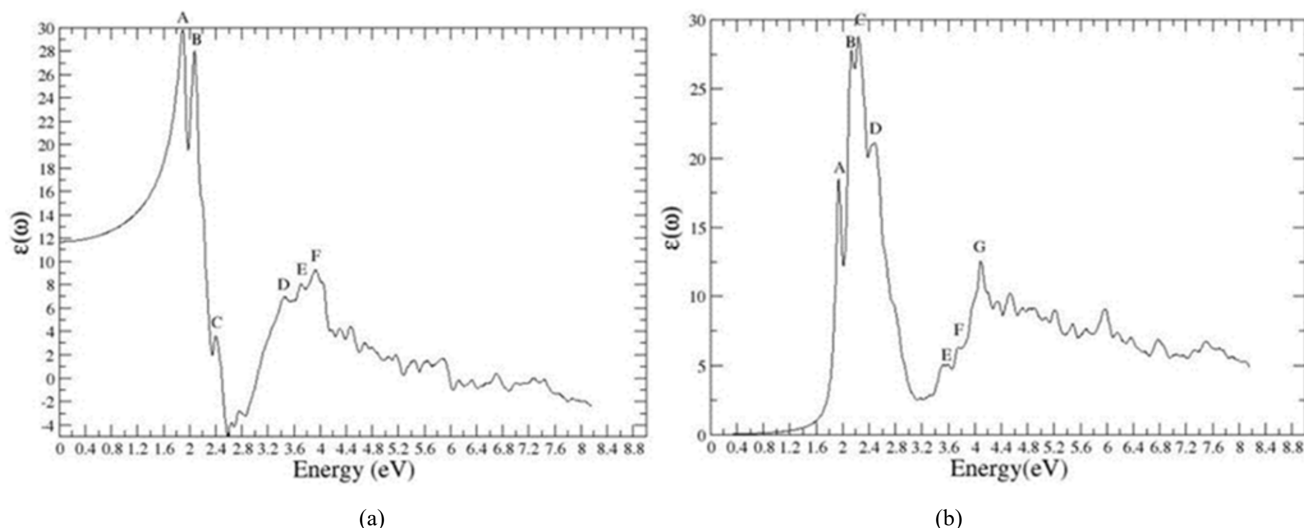

(a) (b)

Fig. 9 The plot of Ɛ(ω) in XX direction for $ZnIn_2Se_4$ (a) real part, (b) imaginary part

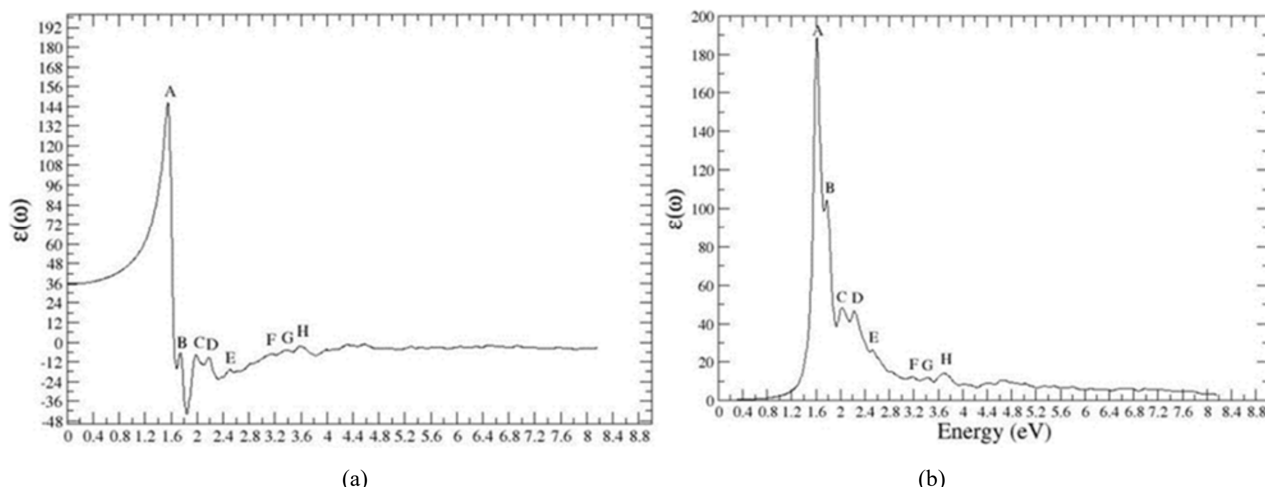

(a) (b)

Fig. 10 The plot of Ɛ(ω) in XX direction for $ZnIn_2Te_4$ (a) real part, (b) imaginary part

V. Conclusion

$ZnIn_2Se_4$ and $ZnIn_2Te_4$ are useful materials because of their range of technological applications. Knowledge of their electronic and optical properties is important. These properties have been investigated in this work via DFT framework. The results from this work agree well with experimental data and the results from previous investigations.

Acknowledgment

The authors thank all those who assisted in the analysis of our data especially the technical staff of Physics Department, Federal University Otuke.

References

[1] S. Ozaki, K. I. Muto, H. Nagata and S. Adachi, (2005). Optical absorption and emission in defect-chalcopyrite semiconductor. J. Appl. Phys. 97, 043507, https://doi.org/1063/1.1845582.

[2] B. H. Dhryv, A. Nowicki, B. H. Patel and V. D Dhamecha, (2015). Memory switching characteristics in amorphous $ZnIn_2Se_4$ thin films, surface. Eng. 31, 556-562.

[3] H. M. Zeyada, M. S. Aziz, A. S. Behairy (2009). Structure formation and mechanisms of DC conduction in thermally evaporated nanocrystallite structure $ZnIn_2Se_4$ thin films, phys. B: condensed maters, vol. 404, Issue 21, pp 3957-3963.

[4] D. K. Dhruv and B. H. Patel (2016). Fabrication and electrical characterization of Al/P-$ZnIn_2Se_4$ thin films schottky diode structure, mater. Sc. Semicond. Process. 54, 29-35, https://doi.org/10/016/j.Mssp.2016.06.012.

[5] A. A. Vaipolin, Y. A. Nikolaev, V. Y. Rud, and E. I. Terukov (2003). Photosensitive structure based on $ZnIn_2Se_4$ single crystals, Semiconductor structures, Interfaces, and Surfaces, Vol. 37, pp 414-416.

[6] Y. Chao, P. Zhuo, N. Li, J. Lai, Y. Yang, Y. Zhang, W. Yang, Y. Du, D. Su, Y. Tan, S. Guo, (2019). Ultra-thin visible-light-driven Mo. Incorporating In_2O_3- $ZnIn_2Se_4$ Z-scheme nano sheet photocatalysts, Adv. Mater. 31(5): el807226, doi:10.1002/adma.201807226.

[7] H. H. Gullui, (2019). Investigation of electrical properties of In/$ZnIn_2Te_4$/n-Si/Ag diode, Bull. Materials. Sc. 42: 89, https://doi.org/10.1007/512034-019-177c-z.

[8] H. P. Trah, and V. Kramer (1985). Crystal structure of Zinc Indium selenide, $ZnIn_2Se_4$ zeitsehrift fur kristallographic crystalline materials, vol 173, number 1-4, pp 199-204, https://doi.org/10.1524/zkri.1985.173.14.199

Open Science Index, Chemical and Materials Engineering Vol:18, No:5, 2024 publications.waset.org/10013650.pdf

[9] R. E. Marsh and W. R. Robinson (1988). On the structure of $ZnIn_2Te_4$, journal of solid state chemistry, vol 73, issue 2, pp 591-592.

[10] C. Razzett, G. Attolini, S. Bini, P. P. Lottici (1992), Synthesis and characterization of the layered compounds in the $ZnIn_2S_4$- $ZnIn_2Se_4$ System, Physical status solid B, vol. 173, issue 2, pp 525-531, https://doi.org/10.1002/pss6.2221730204.

[11] V. Riede, H. Neumann, H. Schwer, V. Kramer, I. Gregora, V. Vorlicek (1993), infrared and Raman spectra of $ZnIn_2S_4$, Cryst. Res. Technol, 28,5,641-645.

[12] L. I. Soliman, M. H. Wasfi, and T. A. Hendia (2000). Thermal properties of Polycrstalline $ZnIn_2Se_4$, Journal of Thermal Analysis and Calorimetry, vol. 59, pp. 971-976, https://doi.org/10.1023/A:101019482987.

[13] H. M. Zeyada, M. S. Aziz and A. S. Behairy (2009), Absorption and dispersion studies of thermally evaporated nano crystallite structure $ZnIn_2Se_4$ thin films, Eur. Phys. J Appl. Phys. 45, 30601, https://doi.org/10.1051/epjap/2009009

[14] P. Babu, K. T. R. Reddy, R. W. Miles (2011). Precursor concentration effect on the properties of $ZnIn_2Se_4$ layers grown by chemical bath deposition, Energy procedia 10, 177-181.

[15] D. K. Dhruv, B. H. Patel, and D. Lakshminarayana (2016). Heterojunction of $ZnIn_2Se_4$ and Si was prepared by flash evaporation technique, Materials Research Innovations, vol. 20, issue 4, https://doi.orn/10.1080/14328917.2015.1131919

[16] A. A. Attia, H. A. M. Ali, G. F. Salem, M. I. Ismail, F. F. Al-Harbi (2017) Analysis of electrical properties of heterojunction based on $ZnIn_2Se_4$, Optical Materials 66,480-486.

[17] S. Khawar, N. A. Noor, A. Malik, B. U. I. Haq, and A. Laref A. (2019). Ab-initio investigations of structure optoelectronic, and thermoelectric properties of AIn_2Se_4 (A = Zn, Cd) spinels, Materials Research Express, Vol 6, number 8, 086308, 2019.

[18] S. M. Patel and M. H. Ali (1987). Growth of $ZnIn_2Te_4$ thin films, Materials Letters, Vol 5, Issue 9, pp 350-356.

[19] S. Ozaki and S. Adachi (2001). Optical properties and electronic band structure of $ZnIn_2Te_4$, Phys. Rev. B. 64, 085208.

[20] T. Suriwong, K. Kurosaki, S. Thongtem, A. Harnwunggmoung, T. Plirdpring, T. Sugahara, Y. Ohishi, H. Muta, and S. Yamanaka (2011). Synthesis and Thermal conductivities of $ZnIn_2Te_4$ and $CdIn_2Te_4$ with defect –chalcopyrite structure, Journal of Alloys and Compounds, Vol 509, Issue 27, pp 7484-7487.

[21] M. Rashid, A. S. Alghamdi, Q. Mahmood, M. Hassan, M. Yaseen, A. Laref (2019) Optoelectronic and thermoelectric hehaviour of XIn_2Te_4 (X = Mg, Zn, and Cd) for energy harvesting application: DFT approach, physica scripta 94(12), Doi:10.1088/1402-4896/ab154f.

[22] A. M. Shakra, M. Fadel, and S. S. Shenouda (2020). Response of electrical and dielectric parameters of $ZnIn_2Te_4$ thin films to temperature and frequency, Physical B: Condensed Matter, Vol. 585, 412082.

[23] B. Ganguli, K. K. Saha, T. Saha-Dasgypta, A. Mookerjee, and A. K. Bhattacharya (2004). Electronic and optical properties of $ZnIn_2Te_4$, Physica B: Condensed Matter Vol. 348, Issue 1-4,pp 382-390.

[24] Y. Ayeb, T. Ouahrani, R. Khenata, A. Reshak, D. Rached D, A. Dou Bouhema, R. Arrar (2010). FP-LAPW investigation of structural, electronics, linear and nonlinear optical properties of $ZnIn_2Te_4$ defect-chalcopyrite, Computational Material Sci., 50, 651-655.

[25] Y. Ayeb, A. Benghia, M. B. Akanoun, R. Arrar, B. Lagoon, and S. Goumri–Said. (2019). Elucidation linear and nonlinear optical properties of defect chalcopyrite compounds $ZnIn_2Te_4$ (X = Al, Ga, In) from electronic transitions, solid state sciences, vol. 87, pp. 39 39-48, https://doi.org/10.1016/j.solid state sciences. 2018.08.002.

[26] S. Reguieg, R. Baghdad, A. Abdiche, M. A. Bezzerrouk, B. Benyoucef, R. Khenata, and S. Bin-Omran. (2017). First–principles study of strucutural, optical, and thermodynamic properties of $ZnIn_2X_4$ (X = Se, Te) compounds with DC or DF structure, Journal of Electronic Materials, Vol 46, No 1, DOI:10.1007/511664-016-4831-8.

[27] B. Wu, G. Wang and J. Hu (2021). First principle study of the vacancy defects in $ZnIn_2Te_4$ and $CdIn_2Te_4$, International Journal of Modern Physics C, Vol .32, Issue 12, 1-12, 2021.

[28] O. Madelung, (2004), Semiconductors: Data hand book, springer, 3rd edition

[29] X. Gonze, J. M. Beuken, R. Caracas, F. Detraux, M. Fuchs, G. M. Rignanese, L. Sindic, M. Verstraete, G. Zerah, F. Jollet, M. Torrent, A. Roy, M. Mikami, Ph. Ghosez, J.-Y. Raty, and D. C. Allan, (2002) First-principles computation of material properties: the Abinit software project, Computational Materials Science 25, 478-492.

[30] X. Gonze, G.-M. Rignanese, M. Verstraete, J.-M. Beuken, Y. Pouillon, R. Caracas, F. Jollet, M. Torrent, G. Zerah, M. Mikami, Ph. Ghosez, M. Veithen, J-Y. Raty, V. Olevano, F. Bruneval, L. Reining, R. Godby, G. Onida, D. R. Hamann, and D. C. Allan, (2005) A brief Introduction to the Abinit software package. Z. Kristallogr. 220, 558-562.

Open Science Index, Chemical and Materials Engineering Vol:18, No:5, 2024 publications.waset.org/10013650.pdf